

## Experimental Report:

### **Nucleation and growth studies of CdS nano-clusters by *in situ* SAXS-WAXS techniques**

CH-1288

F. Meneau

#### **1. Introduction**

Intense activity has been seen over the last decade in the area of preparation of nanometer-sized semiconducting materials using a variety of methods of chemistry. Most of the research is concentrated in the synthesis of semiconducting particles belonging to II-VI and III-V groups of the periodic table since these direct gap materials show significant quantum confinement effects (Alivisatos *et al.*, 1996; Brus *et al.*, 1984; Weller, 1993), the electrical and optical properties varying significantly with particle size (30-100Å). In particular cadmium and zinc based oxides and sulfides have been the subject of interest for this purpose. The ability to tune the physical properties by controlling particle size by the growth conditions can find potential uses in a variety of applications. These materials, prepared by a variety of methods (Duonghong *et al.*, 1982; Kortan *et al.*, 1990; Wark *et al.*, 1997), can be characterized by for instance optical and X-ray spectroscopy (Rockenberger *et al.*, 1997) and X-ray scattering techniques. The latter play a major role in determining the size and shape of the nanometer sized (Aletru *et al.*, 1999; Greaves *et al.*, 2002). Here we report on the investigation of the formation of cadmium sulfide nanoclusters from a solution containing cadmium acetate and thioacetamide. We have performed *in situ* Small Angle X-ray Scattering (SAXS) experiments time-resolved to follow the formation of the monodispersed particles during the reaction between thioacetamide and the salt. The analysis of the SAXS data and the evolution of the particle size and shape with time will be discussed.

#### **2. Experimental methods**

CdS nanoparticles were synthesized in hydrothermal cells by dissolving cadmium acetate [Cd(CH<sub>3</sub>COO)<sub>2</sub>] in distilled water and by subsequently reacting it with thioacetamide (TAA) at several temperatures (room temperature (*RT*), 60°C, 80°C, 100°C and 120°C) and for different period of time (between 12 and 24 hours). The

precipitates were then filtrated, washed in distilled water, in order to remove impurities, and finally dried at 50°C. For the *in situ* experiments, the same liquid mixture was quickly introduced at *RT* into a specially designed *in situ* cell that included 50µm mica as the window material.

Transmission electron microscopy (TEM) were taken with a Hitachi HF 2000 transmission electron microscope equipped with a cold field emission source, using an accelerating voltage of 200 kV.

*In situ* SAXS measurements were carried out at station BM26b, DUBBLE CRG beamline of the ESRF, with an X-ray photon energy of 11.79 keV. The time resolution of 2 minutes/time frame was matched to the speed of the structural development which was on the order of several hours. A photon counting position sensitive area detector was used. Two different sample-detector distances of respectively 1.5 (experiment 1) and 8 meters (experiment 2) were used. This corresponds to scattering vector ranges  $q$ , of respectively 0.034 – 0.623 Å<sup>-1</sup> and 0.005 – 0.08 Å<sup>-1</sup>. The scattering vector ( $q$ -axis) was calibrated with the scattering pattern of silver behenate for the 1.5 m camera and of dry rat-tail collagen for the 8 m one. For each experiment, the required amount of reacting solution was inserted into the cell and the scans were started at time  $t_0$ , which was typically approximately 3 minutes.

A solution of cadmium acetate (CdAc) in distilled water was used for background normalization. The data reduction of the time-resolved SAXS was processed using BSL and XOTOKO programs (Mant, 2002) available at the SRS, Daresbury Laboratory.

#### **3. Results**

It is known cadmium sulfide crystallizes in sphalerite and wurtzite phases, with cubic and hexagonal crystal structures, respectively.

TEM micrographs of CdS nanoparticles, synthesized at 120°C during 15 hours, are shown in Figure 1. The crystal structure of the CdS crystals can be clearly identified as the pure hexagonal phase with no evidence of the cubic one.

Figures 2 a) and b) show stacked time-resolved SAXS intensity,  $I(q)$ , collected with 8 and 1.5 m sample-detector distance, during the reaction of cadmium acetate with thioacetamide.

In both cases a gradual increase in the scattering intensity in the low  $q$  region is observed. In experiment 1 (Figure 2 b)), after about 40 minutes of reaction, a step in the scattering intensity occurs

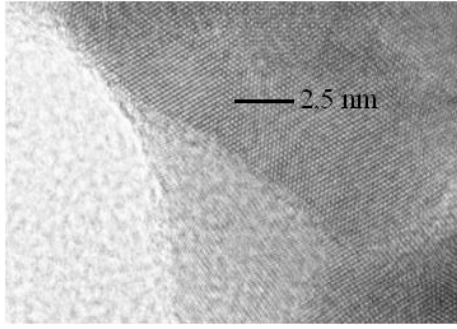


Figure 1: Transmission Electron Microscopy (TEM) of CdS nanoclusters synthesized by a hydrothermal process at 120°C during 15 hours; reacting thioacetamide with cadmium acetate in distilled water.

which suggests change in the growth mechanism is taking place. In experiment 2, from Figure 2 a), it is clear that, as  $I(q)$  increases in the low  $q$  region we observe the appearance of scattering intensity around  $q = 0.04 \text{ \AA}^{-1}$ , which can be attributed to scattering from a dilute distribution of particles. The feature shifts to lower  $q$  values with reaction time, indicating that either the particles increase in size or that the small particles aggregate and therefore form larger structures. After 6 hours of reaction, second and third order maxima become clearly visible (Figure 4). This is typically observed for many systems that represent nucleation and growth processes, which ultimately yields to highly monodispersed particles and rules out an aggregation process.

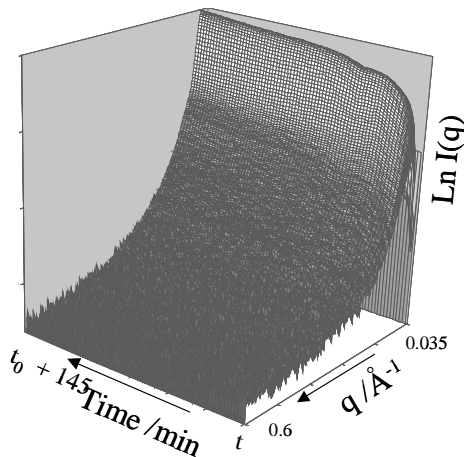
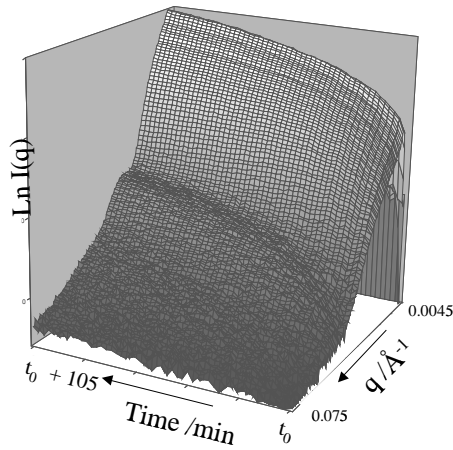


Figure 2: Stacked *in situ* SAXS data recorded with a time resolution of two minutes/time frame during the reaction of thioacetamide with cadmium acetate at room temperature; using the 8 meter camera set-up in picture a) and the 1.5 meter one in b). In both cases the scattering intensity  $I(q)$  in the low  $q$  region is increasing. In a), we observe a step in  $I(q)$  after about 40 minutes of reaction (black arrow). In b) the broad form factor bump around  $q = 0.04 \text{ \AA}^{-1}$  is increasing in intensity and shifts to lower  $q$  values.

## 4. Analysis and Discussion

### 4.1. Particles size and the Guinier region

The intensity of the small angle X-ray scattering,  $I(q)$ , is given by:  $I(q) = NP(q)S(q)$  (1)

where  $N$  is the number of scatterers in solution,  $P(q)$  is the form factor and  $S(q)$  the structure factor. For dilute solutions,  $S(q)$  is a constant and the scattered intensity  $I(q)$  in the low  $q$  region can be approximated by:

$$I(q) = C \exp\left(-\frac{R_g^2 q^2}{3}\right) \quad (2)$$

$C$  is a scaling constant and  $R_g$  is the Guinier radius or radius of gyration, and  $q$  is the scattering vector. By the time measurements commenced ( $t_0$ ), the radius of gyration,  $R_g$ , has reached about 90 Å and is rapidly increasing (Figure 3). At time  $t_0 + 45$  minutes, particles with a radius of gyration of 133 Å are being formed when a change in the slope of the

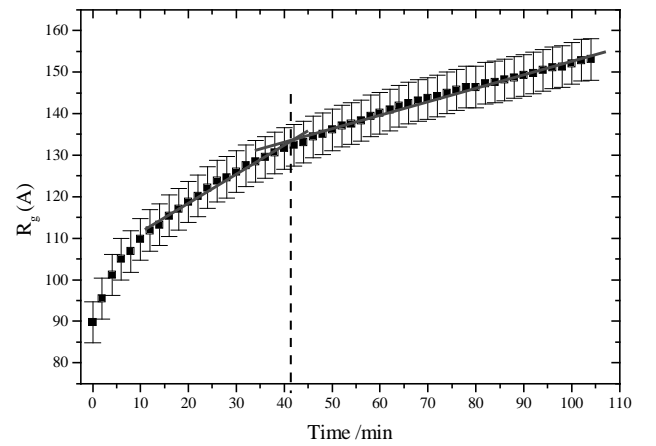


Figure 3: Size development of the Guinier radius  $R_g$ , versus time of reaction.

increase of  $R_g$  is observed. This kink is referred to a change in the growth process. With increasing time, particles finally reach a maximum detectable size with a radius of gyration  $R_g$  of 191 Å after about 6 hours of reaction.

### 4.3 Particles shape and monodispersity

The features observed in experiment 2 (Fig 2 and 4) can be interpreted as the emergence of a form factor in  $I(q)$ . At first a maximum occurs at  $0.04 \text{ \AA}^{-1}$

but after 6 hours of reaction a secondary maximum appears. It is illustrated in Fig. 4. At later stages a third maximum appears.

Since it was difficult to accurately assess the position of the second and third maxima, the position of the first maxima and minima in Fig. 4 were fitted. For the 8m-camera experiment, spherical and cylindrical form factors have been fitted to the whole scattering function. Spherical form factors were used for the first few minutes of the experiment, and at time  $t_0 + 40$  minutes, these were replaced by cylindrical form factors.

Figure 4 illustrates several examples of the form fitting to the data where the agreement shown between the calculated and the experimental graphs is good over the whole dynamic region.

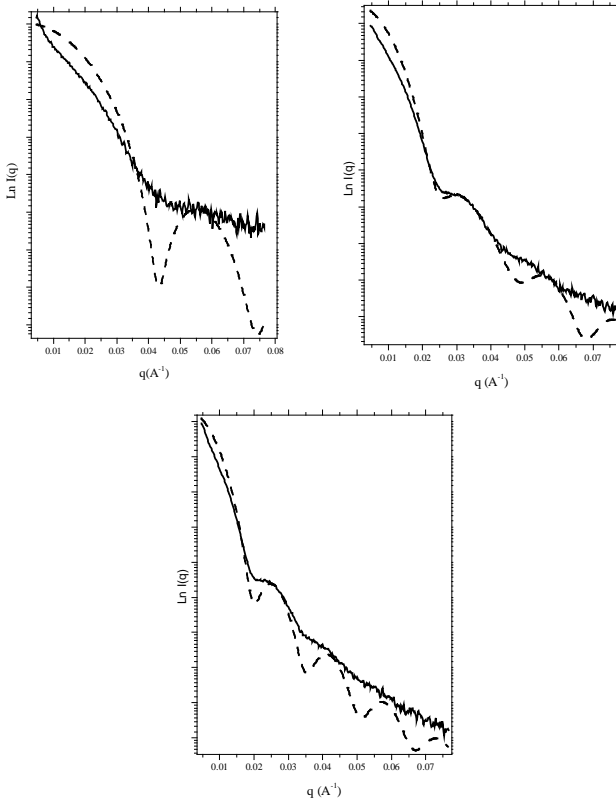


Figure 4: Detailed fits of the form factor, illustrating the cylindrical like shape of the CdS nanoparticles. The fits (dash lines) and the experimental data are in excellent agreement. In a), SAXS profile at time  $t_0$  fitted with a cylindrical function; in b) and c) SAXS profiles at  $t_0 + 2$  hours and  $t_0 + 6$  hours respectively, fitted with a cylindrical function.

The spherical and cylindrical radii  $R_s$  and  $R_c$ , and the cylinder length  $L_c$  are tabulated in Table 1 where they are compared to the Guinier radius  $R_g$  obtained from equation (2).

For spherical particles  $R_g$  is given by:

$$R_g^2 = \frac{3}{5} R_s^2 \quad (3)$$

In the case of cylindrical particles  $R_g$  can be obtained from  $R_c$  and  $L_c$ , using the standard geometric expression:  $R_g^2 = \frac{R_c^2}{2} + \frac{L_c^2}{12}$  (4)

The Guinier radii obtained in this way closely match those deduced from equation (2), as well as the increase in particle size with time. The final value, from the spherical fit is approximately  $10\text{\AA}$  shorter i.e.  $R_g = 81\text{\AA}$  compared to  $90\text{\AA}$  which is expected if the distribution is not fully monodispersed. For the cylindrical fits, the final values are also in good agreement with the experimental ones. However they are slightly larger at the end of the reaction, i.e.  $R_g = 217\text{\AA}$  compared to  $191\text{\AA}$ . This might suggest that even in this case the system may not be perfectly monodispersed in the final stages of growth.

Moreover, it is consistent with the calculations done on zinc sulfides by Hamad *et al*, using interatomic potential based simulations and Density Functional Theory (DFT). Hamad *et al* showed that ZnS, in its hexagonal phase, has a highly anisotropic, cylindrical like shape, with non-polar surfaces on the sides, and polar surfaces closing the cylinder. Our results suggest similar habit formation during the growth of CdS.

### 4.3 The Porod region

In the high  $q$  range of the SAXS, the scattering intensity is given by:

$$I(q) = K_1 + \frac{K_2}{q^\alpha} \quad (5)$$

where  $K_1$  is the thermal background,  $K_2$  is the Porod constant and  $\alpha$  is a parameter influenced by the dimensionality and the surface roughness of the scattering particles.

For a two-phase system, CdS nanoparticles crystallizing out of a water solution, the SAXS invariant  $Q$  is defined by the following expression:

$$Q = \int_{q=0}^{q=\infty} I(q) q^2 dq = x(1-x)(\Delta\rho)^2 \quad (6)$$

where  $\Delta\rho$  is the electron density difference,  $q$  the scattering vector and  $x$  is the fraction of one phase. A maximum is predicted when  $x$  is equal to 0.5, i.e. a volume fraction of 50% for both phases.

$Q$  is also a sensitive measure of the amount of microstructural development in the sample (Glatter *et al*, 1982), and is sensitive both to the volume fractions of the phases present as well as to the electron density contrast between them.  $Q$  is plotted in Figure 5 against the reaction time. For experiment

1, we observe two clear regions, the first one (region 1) from time  $t_0$  to  $t_0 + 40$  minutes and the second one (region 2) from  $t_0 + 40$  minutes until the end of the reaction. These correspond with the switch from spherical to cylindrical crystal growth.

In region 1, the data can be fitted to a 2<sup>nd</sup> order polynomial with a maximum around  $t_0 + 32$  minutes suggesting that at this point equation (6) is obeyed. However our system cannot be considered as a pure two-phase system in the sense that, as the CdS crystallization occurs, the solute changes its concentration and thus the electron density contrast between the two phases is changing. Therefore the invariant  $Q$  can only be used as an indication of the microstructural development. The important feature is the clear step around  $t_0 + 40$  minutes, which is indicating a change in the crystallization process. One has to note that this feature does correspond to the kink (change in slope) previously observed in Figure 4.

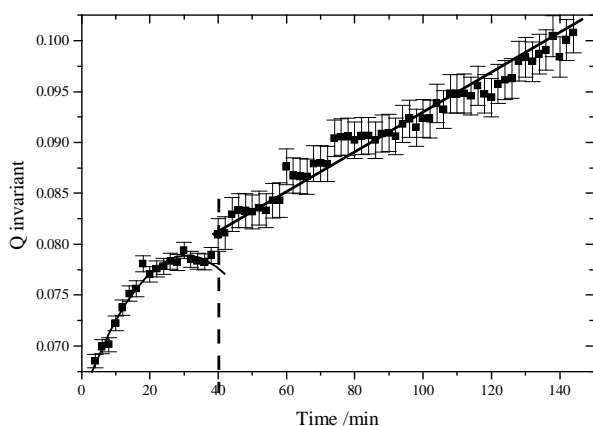


Figure 5: Development of the  $Q$  invariant versus time of reaction.

Since there is a change in the growth rate of the Guinier radii simultaneously with a change in the growth of  $Q$  observed at  $t_0 + 32$  minutes is more properly interpreted as indicating that spherical particles have attained a maximum size and that, by  $t_0 + 40$  minutes, the conversion from spherical to cylindrical growth has started.

## Conclusions

The SAXS and TEM results presented here follow the nucleation and growth of cadmium sulfide nanoparticles and quantify: the crystallites as spherical in the early stages of the reaction, and cylindrical afterwards; monodispersed and with a final average radius  $R_c$  of  $210 \text{ \AA} \pm 20 \text{ \AA}$  and length  $L_c$  of  $550 \text{ \AA} \pm 55 \text{ \AA}$ .

Finally we have shown that time resolved SAXS experiments is a powerful tool for the study of nanoparticle growth in solutions.

## References:

- Aletru, C. Greaves, G. N., Sankar, G., (1999). *Jpn. J. Appl. Phys.* **1** 38: 97-100 Suppl. 1.
- Alivisatos, A. P., (1996). *Science*. **271**, 933.
- Brus, L., (1984). *J. Phys. Chem.* **80**, 4403.
- Duonghong, D. Ramsden, J. J. & Gratzel, M., (1982). *J. Am. Chem. Soc.* **104**, 297.
- Glatter, O. & Krakty, O., (1982). *Small Angle X-Ray Scattering*, Academic Press, New-York.
- Greaves, G. N. Bras, W. Oversluizen, M. & Clark, S. M., (2002). *Faraday. Disc.* **122**, In Press.
- Hamad, S. Cristol, S. & Catlow, C. R. A., (2002). *J. Phys. Chem.* In Press.
- Kortan, A. R. Hull, R. Opila, R. L. Bawendi, M. G. Stiegerwald, M. L. Carroll, P. J. & Brus, L. E., (1990). *J. Am. Chem. Soc.* **112**, 1327.
- Mant, G. R., (2002). Private Communication.
- Rockenberger, J. Troger, L. Kornowski, A. Vossmeier, T. Eychmuller, A. Feldhaus, J. & Weller, H., (1997). *J. Phys. Chem. B.* **101**, 2691-2701.
- Russel, T. P. (1991). *Handbook on Synchrotron Radiation*. Vol 3.
- Wark, M. Kessler, H. & Schulz-Ekloff, G., (1997). *Microporous Materials*, **8**, 241-53.
- Weller, H., (1993). *Angew. Chem., Int. Ed. Engl.* **32**, 41.